LETTER | DECEMBER 13 2023

# Frequency combs in optically injected terahertz ring quantum cascade lasers

Special Collection: State-of-the-Art and Future Directions in Optical Frequency Comb Sources, Enabling Technologies, and Applications

Md Istiak Khan 🗷 💿 ; Zhenyang Xiao; Sadhvikas J. Addamane 💿 ; David Burghoff 💿

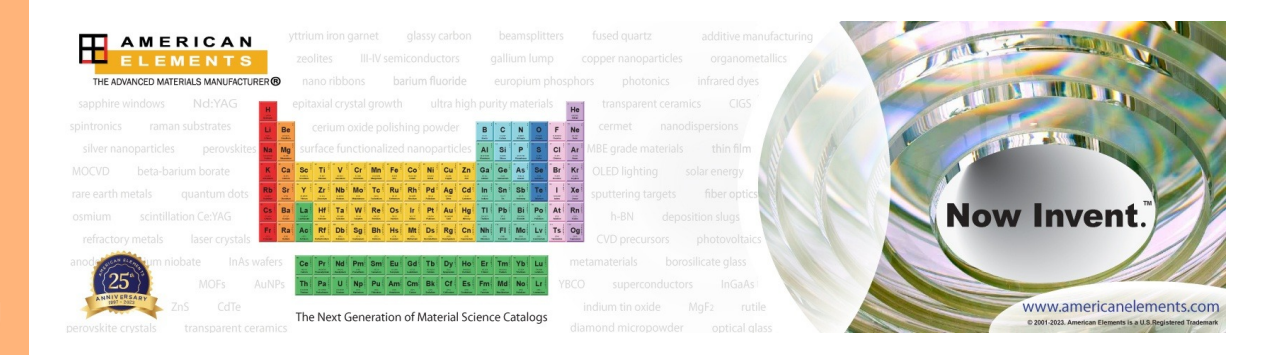


APL Photonics 8, 121302 (2023) https://doi.org/10.1063/5.0173912





CrossMark





## Frequency combs in optically injected terahertz ring quantum cascade lasers

Cite as: APL Photon. 8, 121302 (2023); doi: 10.1063/5.0173912 Submitted: 25 August 2023 • Accepted: 21 November 2023 • Published Online: 13 December 2023









Md Istiak Khan,<sup>1,a)</sup> D Zhenyang Xiao,<sup>1,2</sup> Sadhvikas J. Addamane,<sup>3,4</sup> D and David Burghoff<sup>1,2</sup> D





### **AFFILIATIONS**

- <sup>1</sup> Electrical Engineering, University of Notre Dame, Notre Dame, Indiana 46556, USA
- <sup>2</sup>Electrical and Computer Engineering, University of Texas at Austin, Austin, Texas 78712, USA
- Center for Integrated Nanotechnologies, Sandia National Laboratories, Albuquerque, New Mexico 87123, USA

Note: This paper is part of the APL Photonics Special Topic on State-of-the-Art and Future Directions in Optical Frequency Comb Sources, Enabling Technologies, and Applications.

a) Author to whom correspondence should be addressed: mkhan6@nd.edu

#### **ABSTRACT**

Quantum cascade lasers (QCLs) have emerged as promising candidates for generating chip-scale frequency combs in mid-infrared and terahertz wavelengths. In this work, we demonstrate frequency comb formation in ring terahertz QCLs using the injection of light from a distributed feedback (DFB) laser. The DFB design frequency is chosen to match the modes of the ring cavity (near 3.3 THz), and light from the DFB is injected into the ring QCL via a bus waveguide. By controlling the power and frequency of the optical injection, we show that combs can be selectively formed and controlled in the ring cavity. Numerical modeling suggests that this comb is primarily frequency-modulated in character, with the injection serving to trigger comb formation. We also show that the ring can be used as a filter to control the output of the DFB QCL, potentially being of interest in terahertz photonic integrated circuits. Our work demonstrates that waveguide couplers are a compelling approach for injecting and extracting radiation from ring terahertz combs and offer exciting possibilities for the generation of new comb states in terahertz, such as frequency-modulated waves, solitons, and more.

© 2023 Author(s). All article content, except where otherwise noted, is licensed under a Creative Commons Attribution (CC BY) license (http://creativecommons.org/licenses/by/4.0/). https://doi.org/10.1063/5.0173912

#### I. INTRODUCTION

Integrated chip-scale frequency combs have diverse applications, including communication, frequency synthesis, optical ranging,<sup>3</sup> and gas spectroscopy.<sup>4–9</sup> In the terahertz (THz) and midinfrared (MIR) regions, the primary compact source for generating frequency combs is the quantum cascade laser (QCL). While QCLs do not easily form pulses due to their short gain recovery time, other kinds of combs, such as frequency-modulated (FM) combs, still readily form. 12,13 Within a Fabry-Perot QCL cavity, fast gain dynamics lead to strong spatial hole burning, <sup>14,15</sup> and the asymmetry of the field at the facets gives rise to phase potentials. This nonlinearity is balanced by the cavity dispersion, and this balance enables the generation of phase-coherent FM combs. 15-17

An alternative method for generating frequency combs involves the use of an integrated QCL ring, which could potentially offer additional advantages due to the lack of strong coupling between fields traveling in counterpropagating directions. Additionally, rings' integrated natures and potential for dissipative Kerr soliton generation make them particularly intriguing. Dissipative Kerr solitons are ultra-short pulses capable of propagating through a dispersive, nonlinear medium while retaining their shape and amplitude.18 The generation of solitons relies on a delicate balance between dispersion, Kerr nonlinearity, parametric gain, and cavity loss. 18,21 Recently, THz QCL ring frequency combs have been demonstrated using both defect<sup>14</sup> and defect-free cavities.<sup>22</sup> In a cavity with defects, the ring resonator still produces spatial hole burning (SHB) due to a reflection point within the defect. On the other hand,

<sup>&</sup>lt;sup>4</sup>Sandia National Laboratories, Albuquerque, New Mexico 87185, USA

in a defect-free cavity, the absence of SHB, combined with anomalous group velocity dispersion, enables the generation of solitons in ring QCL microresonators.<sup>23</sup>

All these configurations utilize the ring QCL by itself without the need for external pumps. This letter discusses another approach, incorporating an integrated external source on the chip. We demonstrate that by injecting the microresonator externally, a broadening of the ring spectra is observed, which is consistent with comb formation. Additionally, a bus waveguide is included to facilitate light coupling in and out of the microresonator, resulting in improved power extraction. Although our experiment did not reveal any cavity soliton formation and primarily shows FM comb formation, this design topology has the possibility of generating solitons using schemes similar to those employed in the mid-infrared regime. <sup>18,24–26</sup> Additionally, we demonstrate that the ring can be used to selectively filter the output of the DFB, which could be useful for mode selection on multimode devices.

#### II. DESIGN

Figure 1(a) provides an overview of the fabricated device structure, consisting of three key components: an integrated external

pump in the form of a distributed feedback (DFB) laser, a bus responsible for coupling with the ring QCL, and the ring itself. All three parts are fabricated on the same QCL gain medium, a GaAs/AlGaAs heterostructure, which is designed to offer gain within the frequency range of 2.5 to 4 THz. The DFB laser is biased above its threshold to ensure efficient coupling into the bus and effective pumping of the microresonator. In contrast, the bus is biased at or slightly below the threshold, allowing it to act as highly transparent waveguides rather than active media. The DFB laser is designed to lase at 3.29 THz and is configured as a first-order DFB,<sup>27</sup> ensuring appropriate coupling into the bus. Simulation of the device's eigenmodes was carried out using a commercial finite element method (FEM) solver (COMSOL). The DFB was fabricated with a periodicity of 13.5  $\mu m$ , with each section measuring 6.75  $\mu$ m. Figure 1(b) presents the simulated eigenmodes. The lowest loss eigenmode obtained in our design corresponded to a frequency of 3.29 THz, representing the second (asymmetric) lateral mode.

Ensuring the proper coupling of light between the bus and the microresonator is of utmost importance. This is achieved through careful design considerations and simulations. Specifically, a consistent 2  $\mu$ m gap between the distributed feedback (DFB) laser and the bus is maintained, with the coupling validated through FEM

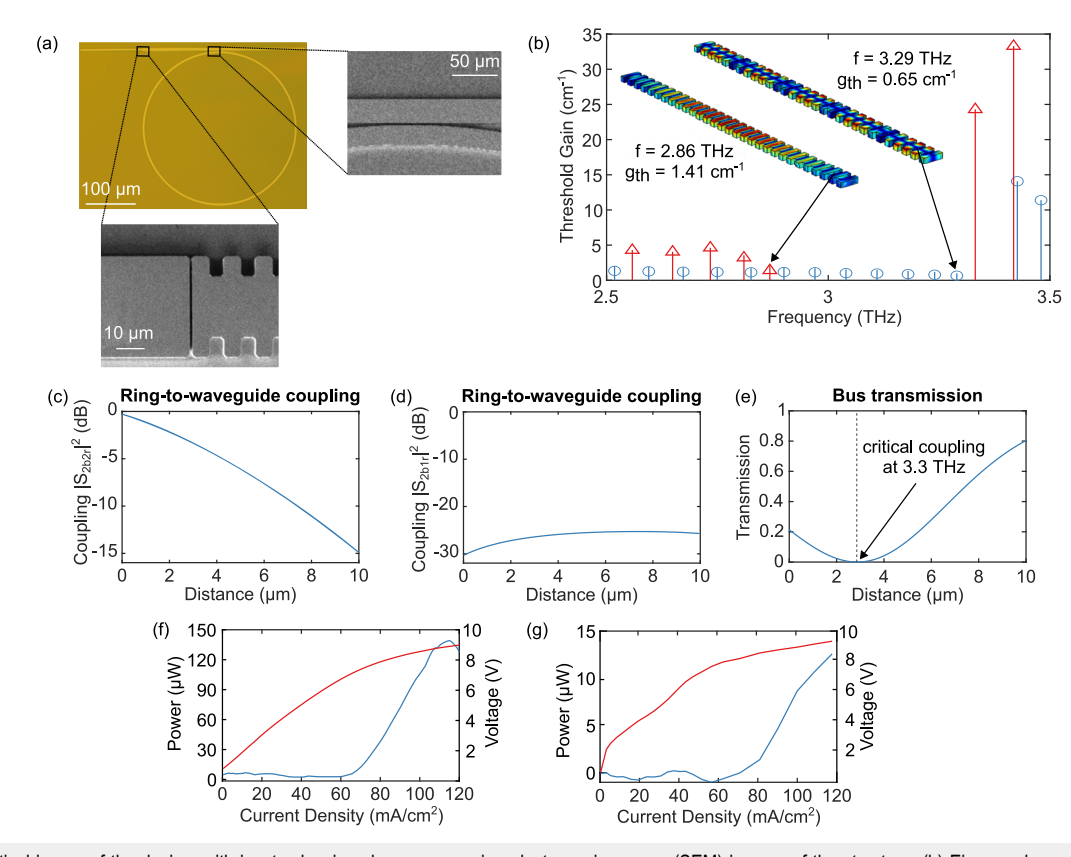


FIG. 1. (a) Optical image of the device, with insets showing close-up scanning electron microscopy (SEM) images of the structure. (b) Eigenmode analysis results of the distributed feedback (DFB) laser showing simulated mode profiles of both even and odd modes. The lowest-threshold mode appears at 3.29 THz. (c) and (d) Variation of the ring-to-waveguide coupling as the distance between the bus and the ring is adjusted. (c) Coupling from the second-order lateral bus mode to the second-order ring mode. (e) Corresponding transmission of a field at resonance. Critical coupling at 3.3 THz occurs at a distance of 3 μm. (f) Calibrated light–current–voltage (LIV) characteristics of the ring. (g) Calibrated LIV curve of the DFB.

simulations. Additionally, coupled mode theory simulations<sup>28</sup> are employed to assess the coupling between the ring and the bus, exploring the impact of different distances on the degree of light coupling into the microresonator. Various configurations are devised to achieve different critical coupling points based on the round-trip loss of the resonator. In the presented study, Fig. 1(e) demonstrates the simulation results, indicating critical coupling at a distance of  $2.6 \mu m$  between the bus and the ring. Notably, in the specific device demonstrated, the distance is set at 2 µm, resulting in an overcoupling. By appropriately biasing the bus and microresonator, we possess the flexibility to adjust the round-trip loss according to our needs. At threshold, the quality factor (Q) of the resonator becomes essentially infinite due to gain clamping. Figures 1(f) and 1(g) present the light-current-voltage characteristics of the ring and the DFB, respectively, as measured using a calibrated detector. The calibrated power curve provides important insight into the power extraction efficiency of our bus waveguide structure. Because our bus is kept below threshold, some of the ring power is lost in transit, and only 120  $\mu$ W is observed outside the bus. The maximum power of the DFB is considerably smaller, only 14  $\mu$ W, implying that the coupling between the bus and DFB is limited. In this work, comb states were observed for injected DFB power levels of around 10  $\mu$ W and ring cavity power levels of 70  $\mu$ W (outside the cavity).

In addition to proper coupling, another crucial factor is the resonance matching between the DFB laser mode and the mode of the ring. Compared with mid-infrared QCLs, THz QCLs offer much less tuning, as the same change in index results in a lower change in frequency. For these DFB lasers, only several hundred MHz of tuning were available. To ensure this resonance was aligned and effectively coupled into the microresonator, we fabricated multiple devices with slight variations in the ring radius. Experimental evidence demonstrated successful light coupling into the microresonator when the modes were matched appropriately. However, one downside of this approach was that rings have large areas when compared with Fabry–Perot lasers, so sweeping the ring radii consumed a significant amount of area on the chip. This necessitated the use of lower-diameter devices. This makes direct detection of the beat note difficult in these structures.

#### III. RESULTS

In our device, when the DFB laser is activated and the bus is maintained slightly below its threshold, we observe a comb-like broadening of the ring spectra. We decided to experimentally verify the proper coupling of light to the ring. To this end, we conducted tuning experiments by varying the ring bias while keeping the DFB bias constant. Throughout the measurements, the bus was held at a threshold, and the light was collected from the output facet of the bus. The presence of a resonant dip in transmission through the bus indicates successful light coupling into the resonator, as shown in Fig. 2(a). We repeat this experiment for different DFB biases and normalize the output by dividing it by the DFB laser power when

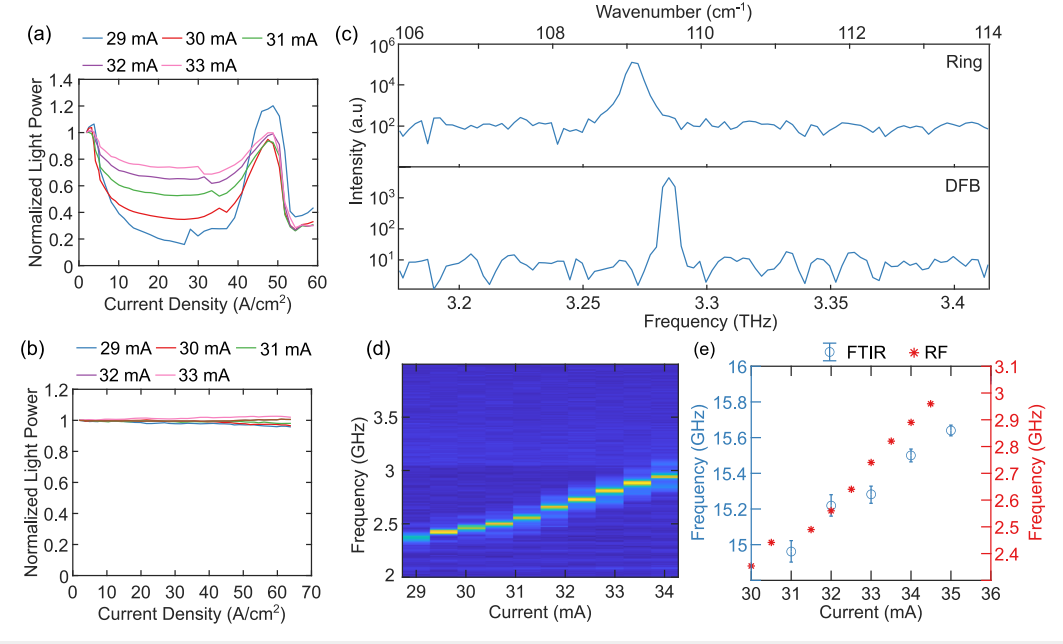


FIG. 2. (a) Normalized output light power collected from the bus as the ring bias is swept up to its threshold. Each curve corresponds to different DFB biases, while the bus is held constant at slightly below its threshold. The DFB and ring modes are matched in this device, leading to a noticeable dip in transmission through the bus. (b) Same experiment conducted on a different device, where the modes of the DFB and the ring are further apart. Unlike in (a), no dip in transmission through the bus is observed. This indicates that the coupling between the DFB and ring modes is not as effective in this device due to the larger separation between the modes. (c) Spectrum of the DFB and ring individually (i.e., when the other device is not on). A difference of 15 GHz is observed. Note that the spectra are taken with different resolutions. (d) Beat note map between the DFB mode and ring mode as the DFB is swept. (e) Tuning of the observed DFB laser frequency, both from the heterodyne beat note and from the optical spectrum. Both show a similar trend with a similar tuning coefficient.

the ring is off. The results reveal a decrease in coupled light as the DFB bias increases.

We also perform a similar experiment on another device where the modes are further apart. In this case, no dip in transmission is observed, except for minor variations within the experimental noise range for different DFB biases. Figure 2(c) displays the spectrum of the DFB mode and the ring modes, obtained individually with the other section turned off while the bus is biased. The modes exhibit a relatively close separation of 15 GHz, with the DFB peak at 3.284 THz and the ring peak at 3.269 THz. However, we were unable to resolve each peak when both were on. To better understand the difference between the mode lines, we examine the heterodyne beat note between the DFB and ring, as measured using a bias tee off the ring. Figure 2(d) presents the beat note map, where we vary the DFB bias while keeping the ring bias constant at 104 mA. As evidenced by the beat note frequencies, the modes progressively separate as the DFB bias current increases. This observation is consistent with the transmission data, which shows reduced light collection from the bus output at higher DFB biases.

Importantly, our experimental results reveal a clear trend of increasing separation between the DFB and ring modes as the DFB bias current is tuned to higher values. This trend is supported by both the beat note frequencies and the transmission data, indicating reduced light coupling into the bus output with higher DFB biases. It is noteworthy that the beat note experiment provides a more accurate representation of the mode separation compared to the individual spectrum data, as it allows simultaneous observation of both modes. The observed linear trend in both the beat note and spectrum experiments further confirms the gradual shift between the two modes.

Figure 3(a) displays the spectrum of the device output. The ring is maintained at a constant bias of 104 mA while the bus is held at threshold. The output spectra are presented as the DFB bias is varied from 30 to 35 mA. Figure 3(b) illustrates the corresponding mode difference between the ring and DFB modes. In the absence of

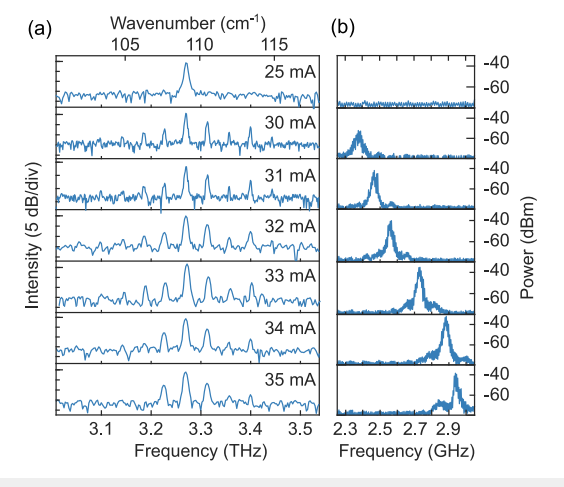


**FIG. 3.** (a) Output spectrum of the ring as the DFB is turned on and swept. The ring spectrum broadens as DFB light is injected, with additional changes occurring as the DFB bias is swept. (b) Corresponding beat note between the DFB and ring modes. As the DFB is detuned from the ring, fewer modes are generated.

injection, the ring operates in a single mode, as depicted in Fig. 2(c). However, in the presence of the pump, we observe a broadening of the ring spectrum. The highest-bandwidth spectrum is obtained when the modes are closest together. As the modes move further apart, a smaller number of modes are observed to be lasing. The broadest bandwidths occur at low injection powers (around  $10~\mu W$  from the DFB, as measured externally), whereas much more power is present in the ring (around  $70~\mu W$ ).

A common method to verify the formation of a comb output is by measuring the beat note on a fast detector. 11,29 A narrow beat note and low phase noise usually indicate comb formation, although additional coherence measurements are usually needed to verify this.<sup>30</sup> However, due to the high mode spacing of this design (required by the sweep), we were unable to perform this experiment on the current device. Instead, we used a superresolution approach to analyze the peak data in the spectrum, zero-padding the interferogram and fitting a parabola to each individual peak to determine the position of the mode peaks to an uncertainty smaller than the instrument resolution.<sup>31</sup> While this approach cannot resolve peaks that are separated by less than the instrument resolution, it can find the centroid to a precision determined by the signal-to-noise ratio. Figure 4(b) presents the peaks of each mode, and Fig. 4(c) shows the difference in frequency between each pair of modes. All of the difference frequencies agree with each other within the error, with the exception of the peak that corresponds to the combined DFB and ring mode. Since the DFB mode and ring modes cannot be resolved in this way, the calculation yields a difference that differs from the others by around 2.5 GHz. This value is essentially a combination

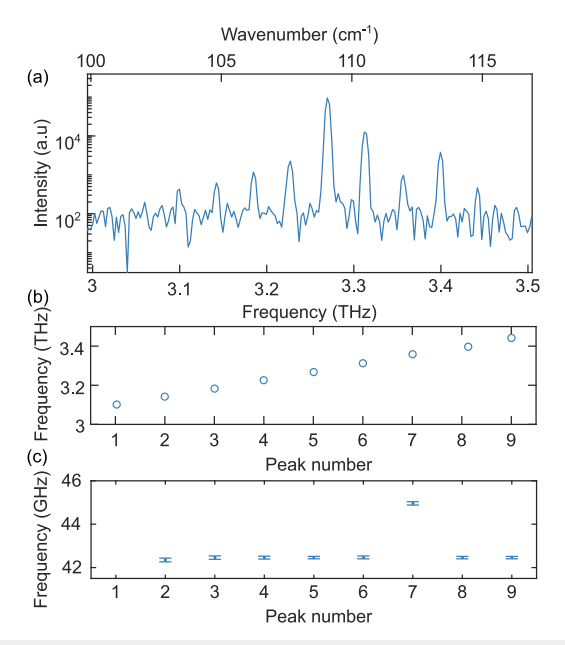


**FIG. 4.** (a) Output spectrum when the DFB is biased at 30 mA and the ring is biased at 104 mA. (b) Observed peaks of each mode in the spectrum. (c) Difference frequency between each successive mode. The difference frequencies are all in agreement, except at the frequency where the DFB is injected (and both spectra are contained within the peak).

of the two signals and is consistent with the observed heterodyne beating.

#### IV. THEORY AND DISCUSSION

To gain further insights into the process of comb formation in ring QCLs, we conducted extensive numerical simulations of our structure. Similar simulations  $^{32}$  have previously been undertaken in both mid-IR  $^{33-35}$  and THz QCL  $^{14,22}$  studies to enhance our comprehension of the underlying dynamics of QCL systems. In this particular investigation, we utilized a master equation formalism previously derived from a two-level Maxwell–Bloch formalism.  $^{15,36,37}$  Essentially, the idea is to replace the full Maxwell–Bloch equations in the adiabatic limit (expanding in  $\partial/\partial t$ ). The result is that light in the cavity is described by a pair of equations for the forward and backpropagating waves  $(A_\pm)$  as

$$\left(\frac{1}{v_g}\frac{\partial}{\partial t} \pm \frac{\partial}{\partial t}\right) A_{\pm} = \left[\frac{i}{2}k''(\omega_0)\frac{\partial^2}{\partial t^2} - \frac{\alpha_\omega}{2} + \frac{g_0}{2}\left(L\left(-i\frac{\partial}{\partial t}\right) - \frac{1}{P_{sat}}\left(|A_{\pm}|^2 + 2|A_{\mp}|^2\right) - \frac{1}{P_{sat}}\left((2T_1 + 3T_2)\frac{\partial A_{\mp}^*}{\partial t}A_{\mp} + \left(T_1 + \frac{5}{2}T_2\right) \times \left(A_{\mp}^*\frac{\partial A_{\mp}}{\partial t} + A_{\mp}^*A_{\mp}\frac{\partial}{\partial t} + A_{\pm}^*A_{\pm}\frac{\partial}{\partial t}\right) + \left(T_1 + \frac{3}{2}T_2\right)A_{\pm}\frac{\partial A_{\pm}^*}{\partial t}\right)\right] A_{\pm}, \tag{1}$$

where the first line contains dispersion  $k''(\omega_0)$  and waveguide loss  $(\alpha_w)$ , the second contains the line shape of the gain medium  $L(\omega)$  and the effect of gain saturation (which reduces the small signal gain  $g_0$  in proportion to the saturation intensity  $P_{sat}$ ), and the last lines contain the five first-order terms resulting from the beating of the

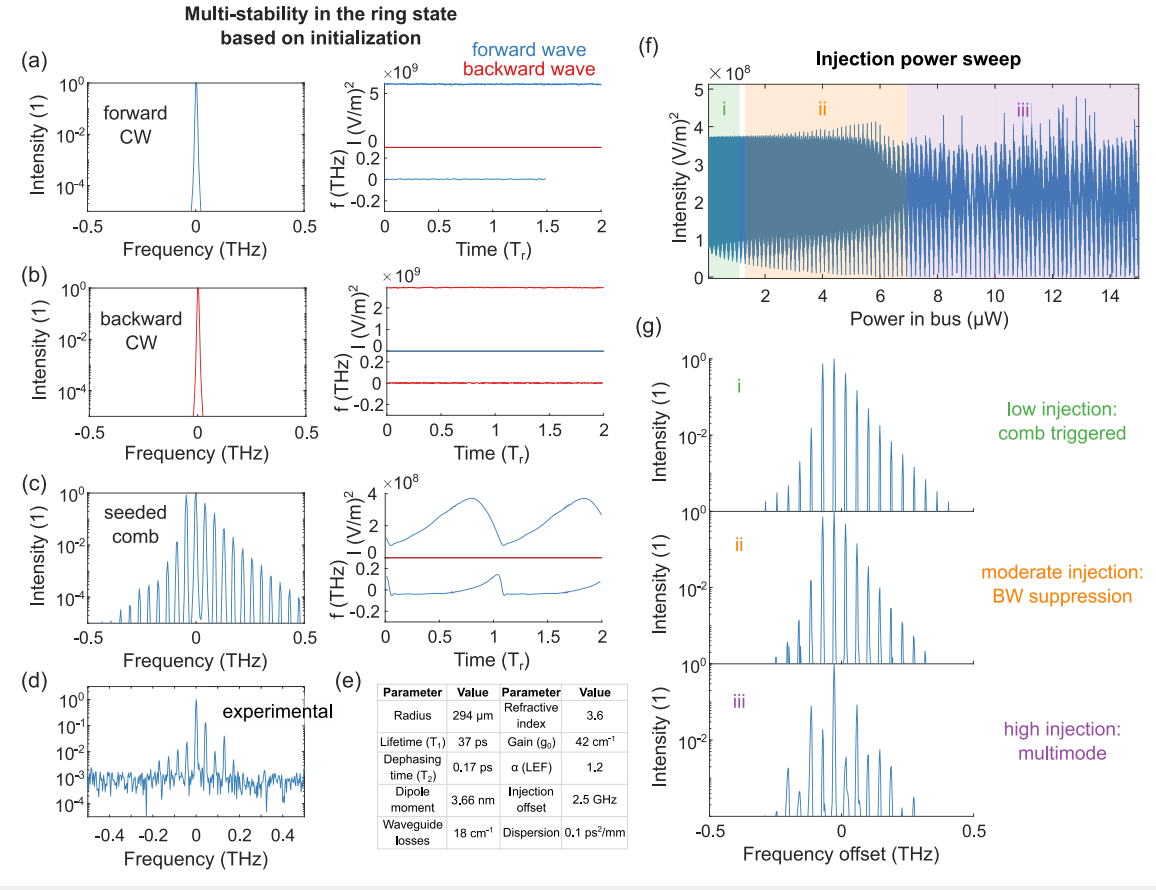


FIG. 5. Numerical simulation of the injected ring QCL based on two-level master equations. (a) For a ring initialized with a sufficiently flat field in the forward direction, only CW light is generated. (b) A similar effect happens in the reverse direction, demonstrating bistability. (c) When the field is initialized with a sufficiently varying field, a comb is instead produced. This comb has a mix of amplitude and frequency modulation. Alternatively, this state can be triggered using optical injection. (d) Experimental spectrum of a low-injection comb from Fig. 4(e) table of parameters for simulations. The small-signal gain (g<sub>0</sub>) was chosen to be 20 cm<sup>-1</sup> above the threshold, and the coupling efficiency θ was chosen to be 50%. (f) Effect of sweeping the power of the injected light on the comb, demonstrating a low-injection regime where comb operation is triggered, a moderate injection regime where the bandwidth is reduced, and a high-injection regime in which the spectrum becomes multimode. (g) Representative spectra of these three regions, showing spectra at 0, 5, and 17 μW of injection, respectively.

gain grating, which in turn depends on the respective upper state and dephasing times of  $T_1$  and  $T_2$ . In this formalism, injection and out-coupling are controlled through boundary conditions using the coupling  $\theta$  [computed in Fig. 1(c)]. Note also that in QCLs, the presence of ultrafast carrier lifetimes often leads to asymmetric gain in the active region,<sup>38</sup> which is modeled using a linewidth enhancement factor<sup>22</sup> incorporated into the small-signal gain  $(g_0 \rightarrow g_0 + i\alpha)$ . The last line couples forwards- and backwards-propagating waves and is responsible for FM comb formation in Fabry-Perot lasers. However, in rings, the coupling between forward- and backward-traveling waves is weak and can only occur by light escaping the system and reflecting within the lossy bus waveguide. As a result, light in one direction will generally dominate, leading to bistability. Figures 5(a) and 5(b) show the impact of initialization on the field. When the field is initialized to a CW wave in the forward direction (and no light is injected), the ring produces only a CW wave in the forward direction. Similar behavior holds true for CW light initialized in the backward direction. This essentially occurs because crosssaturation occurs at twice the strength of self-saturation, promoting one direction at the expense of the other.

In fact, there is additional multistability present. This structure actually predicts the formation of comb states in lasers even without injection, primarily controlled by initialization. Such a state is shown in Fig. 5(c), which is initialized with non-CW light and eventually evolves to a stable comb state with both FM and AM characteristics [simulation parameters are given in Fig. 5(e)]. As it is still unidirectional, it can be modeled by dropping the counterpropagating terms from the master equations and leaving only the self-steepening terms. If  $T_2 \ll T_1$ , this can be further simplified as

$$\left(\frac{1}{\nu_g}\frac{\partial}{\partial t} \pm \frac{\partial}{\partial t}\right) A_{\pm} = \left[\frac{i}{2}k''(\omega_0)\frac{\partial^2}{\partial t^2} - \frac{\alpha_\omega}{2} + \frac{g_0}{2}\right] \times \left(L\left(-i\frac{\partial}{\partial t}\right) - \frac{1}{P_{sat}}|A_{\pm}|^2 + \frac{T_1}{P_{sat}}\right] \\
\left(A_{\pm}^* A_{\pm} \frac{\partial}{\partial t} + A_{\pm} \frac{\partial A_{\pm}^*}{\partial t}\right) A_{\pm}.$$
(2)

For mid-IR rings QCLs, the self-steepening terms are negligible, as the gain recovery time  $T_1$  is typically very short. In this case, there has been significant theoretical interest since the resulting equation is essentially a complex Ginzburg-Landau equation (CGLE), and injection leads to effects such as the formation of solitons and Turing rolls. 33-35 However, for THz QCLs, the situation is quite different, as the gain recovery time is considerably longer. In this case, these dynamics cannot be neglected. In fact, these terms actually dominate in these systems, leading to the production of a novel type of frequency-modulated combs (with significant amplitude modulation resulting from gain curvature). This state is distinct from the FM states present in Fabry-Perot lasers, where the FM nature comes from cross-steepening at the facets. It is nonlinearly chirped, resulting in one side of the spectrum rolling off faster than the other, consistent with our measurements. The dynamics of these systems merit significant theoretical investigation, as the selfsteepening present in lasers is inherently large compared with that of passive materials, and new effects can arise that are not present in other laser systems. Moreover, unlike passive resonators, ring lasers can abide high out-coupling losses—in fact, this is desirable for power extraction.

To investigate the role of the injection, we show in Figs. 5(f) and 5(g) the effect of sweeping the injected signal power on the comb formation. At very low injection powers, the comb is unchanged from the free-running comb that can be present without injection. This suggests that the broadening that occurs when the DFB is turned on comes primarily from the perturbative effect of the injection, shifting the free-running CW state into the comb state. As injection power is increased, the comb begins to narrow, consistent with the measurements, and beyond 7  $\mu$ W of injection, the comb instead enters an incoherent multimode regime, no comb is formed, and the multimode spectrum narrows and becomes chaotic. (At even higher injections, the DFB completely saturates the gain medium and generates a CW output that merely reflects the injection itself.) Furthermore, analytical investigation is needed to fully understand the scaling laws underlying comb formation in this coupled QCL system. Although an analytical theory for ring QCLs has yet to be developed when self-steepening is included, it is likely the case that the dynamics can be governed by a generalized nonlinear Schrödinger equation with a phase potential (as in the case of Fabry-Perot FM combs).

While in this work, we focus on the merits of this structure for comb formation, it has prospects beyond this behavior. For example, as we showed in Fig. 2(a), the presence of the ring coupled to the bus waveguide can be used to make frequency-selective filters, potentially of value in future terahertz photonic integrated circuits. Additionally, such a structure could, in principle, be used to implement nonlinear elements, primarily by exploiting the nonlinear properties of the ring.<sup>39</sup> Future efforts will primarily focus on optimizing the device design to expand the DFB tuning range and minimize the need for sweeping, facilitating smaller free spectral ranges and enabling direct measurements of the intermode beat note. Additionally, although the bus in this system is lossy, we estimate that as much as 25% of the incident injected light could reflect off the end facet and be reinjected into the ring in the backward direction, creating unwanted spatial hole burning that is difficult to model. Although the backscattered light experiences higher losses due to the increased cross-saturation, it could be suppressed even further through the use of tapes or inverse-designed facets<sup>40</sup> that could lower the reflectivity.

#### V. CONCLUSION

In this work, we presented a device designed to investigate comb formation in a ring terahertz quantum cascade laser system. The device consists of three components, all fabricated from the same QCL material. The DFB laser is used to inject a single-mode frequency into the ring QCL, and a long bus waveguide facilitates the coupling of light from the DFB laser to the microresonator and enables efficient light extraction at the output facet. Our results confirmed the broadening of the ring spectrum and the emergence of additional lasing modes upon injection of light from the DFB laser. Although direct beat note measurements were not feasible in this work, the observed broadening of the ring spectra and the agreement in the difference frequencies between the modes strongly indicate the formation of a frequency comb. The conducted numerical simulations also exhibit moderate agreement with the observed data.

Given appropriate design and development, these structures hold the potential to be a flexible platform for generating a variety of comb states.

#### **ACKNOWLEDGMENTS**

This work was supported by Air Force Office of Scientific Research (AFOSR) Grant No. FA9550-20-1-0192. D.B. also acknowledges support from the Gordon and Betty Moore Foundation through Grant No. GBMF11446, the Office of Naval Research (ONR) under Grant No. N00014-21-1-2735, and the National Science Foundation (NSF) under Grant No. ECCS-2046772. This work was performed, in part, at the Center for Integrated Nanotechnologies, an Office of Science User Facility operated for the U.S. Department of Energy (DOE) Office of Science. Sandia National Laboratories is a multimission laboratory managed and operated by National Technology and Engineering Solutions of Sandia, LLC, a wholly owned subsidiary of Honeywell International, Inc., for the U.S. DOE's National Nuclear Security Administration under Contract No. DE-NA-0003525. The views expressed in the article do not necessarily represent the views of the U.S. DOE or the United States Government.

#### **AUTHOR DECLARATIONS**

#### **Conflict of Interest**

The authors have no conflicts to disclose.

#### **Author Contributions**

Md Istiak Khan: Formal analysis (lead); Investigation (lead); Methodology (lead); Software (equal); Writing – original draft (lead); Writing – review & editing (equal). Zhenyang Xiao: Investigation (supporting); Methodology (supporting). Sadhvikas J. Addamane: Methodology (supporting); Resources (equal). David Burghoff: Conceptualization (lead); Software (equal); Supervision (lead); Writing – review & editing (equal).

#### **DATA AVAILABILITY**

The data that support the findings of this study are available from the corresponding author upon reasonable request.

#### **REFERENCES**

- <sup>1</sup>P. Marin-Palomo, J. N. Kemal, M. Karpov, A. Kordts, J. Pfeifle, M. H. P. Pfeiffer, P. Trocha, S. Wolf, V. Brasch, M. H. Anderson, R. Rosenberger, K. Vijayan, W. Freude, T. J. Kippenberg, and C. Koos, "Microresonator-based solitons for massively parallel coherent optical communications," Nature **546**(7657), 274–279 (2017).
- <sup>2</sup>D. T. Spencer, T. Drake, T. C. Briles, J. Stone, L. C. Sinclair, C. Fredrick, Q. Li, D. Westly, B. R. Ilic, A. Bluestone, N. Volet, T. Komljenovic, L. Chang, S. H. Lee, D. Y. Oh, M.-G. Suh, K. Y. Yang, M. H. P. Pfeiffer, T. J. Kippenberg, E. Norberg, L. Theogarajan, K. Vahala, N. R. Newbury, K. Srinivasan, J. E. Bowers, S. A. Diddams, and S. B. Papp, "An optical-frequency synthesizer using integrated photonics," Nature 557(7703), 81–85 (2018).

- <sup>3</sup>J. Riemensberger, A. Lukashchuk, M. Karpov, W. Weng, E. Lucas, J. Liu, and T. J. Kippenberg, "Massively parallel coherent laser ranging using a soliton microcomb," Nature 581(7807), 164–170 (2020).
- <sup>4</sup>G. Villares, A. Hugi, S. Blaser, and J. Faist, "Dual-comb spectroscopy based on quantum-cascade-laser frequency combs," Nat. Commun. 5(1), 5192 (2014).
   <sup>5</sup>A. Shams-Ansari, M. Yu, Z. Chen, C. Reimer, M. Zhang, N. Picqué, and M.
- <sup>5</sup>A. Shams-Ansari, M. Yu, Z. Chen, C. Reimer, M. Zhang, N. Picqué, and M. Lončar, "Thin-film lithium-niobate electro-optic platform for spectrally tailored dual-comb spectroscopy," Commun. Phys. 5(1), 88 (2022).
- <sup>6</sup>N. Picqué and T. W. Hänsch, "Frequency comb spectroscopy," Nat. Photonics 13(3), 146–157 (2019).
- <sup>7</sup>A. Schliesser, M. Brehm, F. Keilmann, and D. W. van der Weide, "Frequency-comb infrared spectrometer for rapid, remote chemical sensing," Opt. Express 13(22), 9029–9038 (2005).
- <sup>8</sup>D. J. Benirschke, N. Han, and D. Burghoff, "Frequency comb ptychoscopy," Nat. Commun. **12**(1), 4244 (2021).
- <sup>9</sup>D. Burghoff, N. Han, and J. H. Shin, "Generalized method for the computational phase correction of arbitrary dual comb signals," Opt. Lett. **44**(12), 2966–2969 (2019).
- <sup>10</sup>J. Faist, F. Capasso, D. L. Sivco, C. Sirtori, A. L. Hutchinson, and A. Y. Cho, "Quantum cascade laser," Science 264(5158), 553–556 (1994).
- <sup>11</sup>J. Faist, G. Villares, G. Scalari, M. Rösch, C. Bonzon, A. Hugi, and M. Beck, "Quantum cascade laser frequency combs," Nanophotonics 5(2), 272–291 (2016).
- <sup>12</sup>A. Forrer, Y. Wang, M. Beck, A. Belyanin, J. Faist, and G. Scalari, "Self-starting harmonic comb emission in THz quantum cascade lasers," Appl. Phys. Lett. **118**(13), 131112 (2021).
- <sup>13</sup>D. Kazakov, M. Piccardo, Y. Wang, P. Chevalier, T. S. Mansuripur, F. Xie, C. Zah, K. Lascola, A. Belyanin, and F. Capasso, "Self-starting harmonic frequency comb generation in a quantum cascade laser," Nat. Photonics 11(12), 789–792 (2017).
- <sup>14</sup>M. Jaidl, N. Opačak, M. A. Kainz, S. Schönhuber, D. Theiner, B. Limbacher, M. Beiser, M. Giparakis, A. M. Andrews, G. Strasser, B. Schwarz, J. Darmo, and K. Unterrainer, "Comb operation in terahertz quantum cascade ring lasers," Optica 8(6), 780–787 (2021).
- <sup>15</sup>N. Opačak and B. Schwarz, "Theory of frequency-modulated combs in lasers with spatial hole burning, dispersion, and Kerr nonlinearity," Phys. Rev. Lett. **123**(24), 243902 (2019).
- <sup>16</sup>D. Burghoff, "Unraveling the origin of frequency modulated combs using active cavity mean-field theory," Optica 7(12), 1781–1787 (2020).
- <sup>17</sup> M. Piccardo and F. Capasso, "Laser frequency combs with fast gain recovery: Physics and applications," Laser Photonics Rev. 16(2), 2100403 (2022).
- <sup>18</sup>T. J. Kippenberg, A. L. Gaeta, M. Lipson, and M. L. Gorodetsky, "Dissipative Kerr solitons in optical microresonators," Science 361(6402), eaan8083 (2018).
- <sup>19</sup>F. Leo, S. Coen, P. Kockaert, S.-P. Gorza, P. Emplit, and M. Haelterman, "Temporal cavity solitons in one-dimensional Kerr media as bits in an all-optical buffer," Nat. Photonics 4(7), 471–476 (2010).
- <sup>20</sup>L. A. Lugiato, "Introduction to the feature section on cavity solitons: An overview," IEEE J. Quantum Electron. **39**(2), 193–196 (2003).
- <sup>21</sup>B. Meng, M. Singleton, J. Hillbrand, M. Franckié, M. Beck, and J. Faist, "Dissipative Kerr solitons in semiconductor ring lasers," Nat. Photonics **16**(2), 142–147 (2022).
- <sup>22</sup> M. Jaidl, N. Opačak, M. A. Kainz, D. Theiner, B. Limbacher, M. Beiser, M. Giparakis, A. M. Andrews, G. Strasser, B. Schwarz, J. Darmo, and K. Unterrainer, "Silicon integrated terahertz quantum cascade ring laser frequency comb," Appl. Phys. Lett. 120(9), 091106 (2022).
- <sup>23</sup>P. Micheletti, U. Senica, A. Forrer, S. Cibella, G. Torrioli, M. Frankié, M. Beck, J. Faist, and G. Scalari, "Terahertz optical solitons from dispersion-compensated antenna-coupled planarized ring quantum cascade lasers," Sci. Adv. 9(24), eadf9426 (2023).
- <sup>24</sup>T. Herr, V. Brasch, J. D. Jost, C. Y. Wang, N. M. Kondratiev, M. L. Gorodetsky, and T. J. Kippenberg, "Temporal solitons in optical microresonators," Nat. Photonics **8**(2), 145–152 (2014).
- <sup>25</sup>C. Joshi, J. K. Jang, K. Luke, X. Ji, S. A. Miller, A. Klenner, Y. Okawachi, M. Lipson, and A. L. Gaeta, "Thermally controlled comb generation and soliton modelocking in microresonators," Opt. Lett. 41(11), 2565–2568 (2016).

- <sup>26</sup>V. Brasch, M. Geiselmann, T. Herr, G. Lihachev, M. H. P. Pfeiffer, M. L. Gorodetsky, and T. J. Kippenberg, "Photonic chip-based optical frequency comb using soliton Cherenkov radiation," Science 351(6271), 357–360 (2016).
- <sup>27</sup>B. S. Williams, S. Kumar, Q. Hu, and J. L. Reno, "Distributed-feedback terahertz quantum-cascade lasers with laterally corrugated metal waveguides," Opt. Lett. **30**(21), 2909–2911 (2005).
- <sup>28</sup>H. A. Haus and W. Huang, "Coupled-mode theory," Proc. IEEE **79**(10), 1505–1518 (1991).
- <sup>29</sup>D. Burghoff, T.-Y. Kao, N. Han, C. W. I. Chan, X. Cai, Y. Yang, D. J. Hayton, J.-R. Gao, J. L. Reno, and Q. Hu, "Terahertz laser frequency combs," Nat. Photonics 8(6), 462–467 (2014).
- <sup>30</sup>D. Burghoff, Y. Yang, D. J. Hayton, J.-R. Gao, J. L. Reno, and Q. Hu, "Evaluating the coherence and time-domain profile of quantum cascade laser frequency combs," Opt. Express 23(2), 1190–1202 (2015).
- <sup>31</sup> M. Rösch, G. Scalari, M. Beck, and J. Faist, "Octave-spanning semiconductor laser," Nat. Photonics **9**(1), 42–47 (2015).
- <sup>32</sup>C. Silvestri, X. Qi, T. Taimre, K. Bertling, and A. D. Rakić, "Frequency combs in quantum cascade lasers: An overview of modeling and experiments," APL Photonics 8(2), 020902 (2023).
- <sup>33</sup>L. Columbo, M. Piccardo, F. Prati, L. A. Lugiato, M. Brambilla, A. Gatti, C. Silvestri, M. Gioannini, N. Opačak, B. Schwarz, and F. Capasso, "Unifying frequency combs in active and passive cavities: Temporal solitons in externally driven ring lasers," Phys. Rev. Lett. 126(17), 173903 (2021).

- <sup>34</sup>F. Prati, M. Brambilla, M. Piccardo, L. L. Columbo, C. Silvestri, M. Gioannini, A. Gatti, L. A. Lugiato, and F. Capasso, "Soliton dynamics of ring quantum cascade lasers with injected signal," Nanophotonics **10**(1), 195–207 (2020).
- <sup>35</sup>F. Prati, L. A. Lugiato, A. Gatti, L. Columbo, C. Silvestri, M. Gioannini, M. Brambilla, M. Piccardo, and F. Capasso, "Global and localised temporal structures in driven ring quantum cascade lasers," Chaos, Solitons Fractals 153, 111537 (2021).
- <sup>36</sup>L. Humbard and D. Burghoff, "Analytical theory of frequency-modulated combs: Generalized mean-field theory, complex cavities, and harmonic states," Opt. Express 30(4), 5376–5401 (2022).
- <sup>37</sup>M. Piccardo, B. Schwarz, D. Kazakov, M. Beiser, N. Opačak, Y. Wang, S. Jha, J. Hillbrand, M. Tamagnone, W. T. Chen, A. Y. Zhu, L. L. Columbo, A. Belyanin, and F. Capasso, "Frequency combs induced by phase turbulence," Nature 582(7812), 360–364 (2020).
- <sup>38</sup>N. Opačak, S. D. Cin, J. Hillbrand, and B. Schwarz, "Frequency comb generation by Bloch gain induced giant Kerr nonlinearity," Phys. Rev. Lett. **127**(9), 093902 (2021).
- <sup>39</sup>D. Kazakov, T. P. Letsou, M. Beiser, Y. Zhi, N. Opačak, M. Piccardo, B. Schwarz, and F. Capasso, "Semiconductor ring laser frequency combs with active directional couplers," arXiv:2206.03379 (2022).
- <sup>40</sup>U. Senica, S. Gloor, P. Micheletti, D. Stark, M. Beck, J. Faist, and G. Scalari, "Broadband surface-emitting THz laser frequency combs with inverse-designed integrated reflectors," APL Photonics 8(9), 096101 (2023).